CARBON 50 (2012) 1355–1362

Available at www.sciencedirect.com

SciVerse ScienceDirect

journal homepage: www.elsevier.com/locate/carbon

Nitrogen-doping of chemically reduced mesocarbon microbead oxide for the improved performance of lithium ion batteries

Pengxian Han, Yanhua Yue, Lixue Zhang, Hongxia Xu, Zhihong Liu, Kejun Zhang, Chuanjian Zhang, Shanmu Dong, Wen Ma, Guanglei Cui *

Qingdao Institute of Bioenergy and Bioprocess Technology, Chinese Academy of Sciences, Qingdao 266101, PR China

ARTICLE INFO

Article history:
Received 5 August 2011
Accepted 7 November 2011
Available online 15 November 2011

ABSTRACT

Nitrogen was doped into chemically-reduced mesocarbon microbead oxide (CR-MCMBO) through simple annealing in ammonia at 800 °C, and the Li-ion storage properties of the prepared nitrogen-doped CR-MCMBO (NR-MCMBO) was studied. It was found that NR-MCMBO shows a highly reversible capacity of 762 mAh g^{-1} at 20 mA g^{-1} during the first charge process, which is much higher than that of the pristine MCMB (289 mAh g^{-1}), and the specific capacity of NR-MCMBO still had a value of 535 mAh g^{-1} after 200 cycles. When the current density reaches 1000 mA g^{-1}, the specific capacity of NR-MCMBO is 388 mAh g^{-1}. The high reversible capacity of NR-MCMBO is attributed to the high amount of pyridinic nitrogen and the large number of defects induced by oxidation and nitrogen-doping. Moreover, the open pores constituted by graphene-like nanoplatelets on the spherical NR-MCMBO surface facilitate the diffusion of Li ions.

1. Introduction

Lithium ion batteries (LIBs) are currently the dominant power source for portable electronic devices and electrical/hybrid vehicles [1–3]. For an anode material, graphite can be reversibly charged and discharged under intercalation potentials with a theoretical capacity of 372 mAh g^{-1} [4–7], and is usually employed as the commercial electrode material in LIBs. However, for its future applications in vehicles and high energy storage, it is necessary to dramatically enhance the specific capacity. Recently, intensive research efforts have been performed to explore new electrode materials with higher energy and power capability [8–10].

As host materials for lithium storage, nitrogen-doped carbon materials have received much attention in recent years [11–13]. It has been established that nitrogen-doping could modify the electronic properties of the carbon graphitic network since nitrogen possesses roughly the same atomic radius as carbon. Experimental and theoretical investigations have demonstrated that the nitrogen atoms incorporated in the matrix of carbon could generate a large amount of defects and withdraw electrons from carbon atoms because of the higher electronegativity of N, and thus facilitate the intercalation of Li^+ [14]. Hence, it can be expected that the energy storage capability of LIBs with nitrogen-doping carbon as the anode material would be improved.

Mesocarbon microbeads (MCMBs) are known to be one of the most important carbonaceous anode materials in LIBs [15–19]. MCMB oxide (MCMBO) could keep its spherical shape under mild oxidation by modified Hummers method [20,21], and after chemical reduction treatment, the surface of the prepared chemically-reduced MCMBO (CR-MCMBO) generated a large amount of open pores between graphene-like nanoplatelets. Such porous texture would offer the chemistry

* *Corresponding author:* Fax: +86 532 80662744.
E-mail address: cuigl@qibebt.ac.cn (G. Cui).
0008-6223/$ - see front matter
doi:10.1016/j.carbon.2011.11.007

and structure to store lithium ions, and the pore-transport system would ensure the accessibility of those sites by lithium ions [22]. Accordingly, the unique structure of CR-MCMBO as anode materials may contribute to good rate performance and cycling stability of LIBs.

Furthermore, studies on the nitrogen-doped CR-MCMBO (NR-MCMBO) as anode materials are rare until now. Hence, it is fundamentally interesting to investigate how nitrogen-doping in NR-MCMBO affect the Li storage in comparison with the pristine MCMBs and CR-MCMBO. With this motivation, we synthesized NR-MCMBO materials through heat treatment in ammonia by using MCMBs as precursors (Fig. 1), and then the feasibility of NR-MCMBO as advanced anode materials of LIBs was investigated.

2. Experimental

2.1. Preparation of MCMBO

MCMBO was prepared by a modified Hummers method [20,21]. Typically, 1 g of graphitic MCMB powder (Shanshan Tech, Shanghai) and 0.5 g of sodium nitrate were added into 23 ml concentrated H_2SO_4 in an ice-bath with drastic agitation, and then 3 g potassium permanganate was slowly added into the mixture. After that, the mixture was transferred into the water bath and kept at room temperature for 50 min. Then 46 ml of de-ionized (DI) water was slowly added which caused the temperature increased to 98 °C, and the mixture was maintained at this temperature for 15 min. The resultant bright yellow suspension was diluted and further treated by 3 ml of H_2O_2 (30%), followed by centrifugation. The addition of H_2O_2 was to reduce residual permanganate to soluble manganese ions. The precipitate was washed repeatedly by 5% HCl and DI water. It is worth noting that the overall preparation process of MCMBO was processed without ultrasonic treatment. The resultant MCMBO was dried at 50 °C in vacuum.

MCMBO was chemically reduced in an aqueous solution (60 ml) of hydrazine monohydrate (100 μl, 2 mmol) at 80 °C for 24 h. The black precipitate was centrifuged, washed with deionized water, and dried at 60 °C in vacuum. Thus CR-MCMBO was obtained.

CR-MCMBO was thermally treated at 800 °C for 5 h in a tube furnace under reactive atmosphere of ammonia with a heating rate of 3 °C min^{-1}. Thus NR-MCMBO was obtained.

For comparison, MCMBO was thermally reduced by heat treatment at 800 °C for 5 h in an N_2 atmosphere with a heating rate of 3 °C min^{-1}. Thus HR-MCMBO was obtained.

In order to improve the first coulomic efficiency, carbon coated NR-MCMBO was also prepared (Supporting Information, preparation of carbon coated NR-MCMBO).

2.2. Sample characterization

Morphological and structural information was obtained from field emission scanning electron microscopy (SEM, HITACHI S-4800). The specific surface area and porous characteristics of the samples were determined with an automated gas adsorption apparatus (Micromeritics, ASAP 2020) using liquid nitrogen adsorption at 77 K. X-ray photoelectron spectroscopy (XPS) data was obtained with an ESCALab220i-XL electron spectrometer from VG Scientific using a 300 W Al K_α radiation. The base pressure was about 3×10^{-9} mbar. After subtracting of the base line (Shirley-type), curve fitting was performed by using the nonlinear least-squares algorithm through a mixed Gaussian/Lorenzian peak shape of variable proportion. Resonance Raman spectra were recorded on a JY HR800 Raman spectrophotometer (Horiba Jobin Yvon, France) with 532 nm diode laser excitation. X-ray diffraction (XRD) patterns were recorded in a Bruker-AXS Micro-diffractometer (D8 ADVANCE) with Cu K_α radiation (λ = 1.5406 nm).

2.3. Electrochemical measurements

The electrochemical properties of MCMBs, HR-MCMBO, CR-MCMBO and NR-MCMBO as anode materials of LIBs were evaluated by galvanostatic charge/discharge technique. The test electrodes were prepared by mixing 85 wt.% active material with 10 wt.% conductive carbon black (super P) as a conductive agent and 5 wt.% polyvinylidene fluoride (PVDF) dissolved in *N*-methyl-2-pyrrolidone (NMP) as a binder to form a slurry, which was then coated onto a copper foil, pressed and dried under vacuum at 120 °C for 12 h. Coin cells were finally assembled in an argon-filled glovebox with MCMBs, HR-MCMBO, CR-MCMBO and NR-MCMBO as test electrodes, metallic lithium as the counter/reference electrode, 1 M $LiPF_6$ in ethylene carbonate (EC) and dimethyl carbonate (DMC) (EC/DMC, 1:1 vol) as electrolyte, and Celgard 2400 polypropylene as a separator. Charge/discharge measurements were carried out galvanostatically at various current densities over a voltage range of 0.005–3 V (vs. Li/Li^+) using a battery test system (LAND CT2001A model, Wuhan Jinnuo Electronics Ltd.). The diameter of the electrodes was 1.4 mm (Fig. S1). The thickness of the electrodes was measured by a micrometer (Fig. S2). Thus the volume of the active materials loaded on copper foil was obtained. Finally, the volumetric capacity was calculated according to Formula (1):

$$\text{Volumetric capacity } (\text{mAh cm}^{-3}) = \frac{\text{Gravimetric capacity}(\text{mAh g}^{-1}) * M_{\text{active materials}}\ (\text{g})}{V_{\text{active materials}}\ (\text{cm}^3)} \quad (1)$$

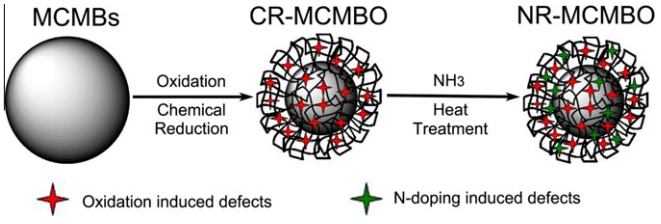

Fig. 1 – Schematic of CR-MCMBO and NR-MCMBO prepared from MCMBs.

Cyclic voltammograms (CV) were tested using Zahner Ennium Electrochemical Workstation (ZAHNER-Elektrik GmbH & Co. KG, Germany) at a scanning rate of 0.1 mV s^{-1} between 0.005 and 3 V. Electrochemical impedance spectroscopy (EIS) measurement was also performed using the Zahner Ennium Electrochemical Workstation by applying an AC voltage of 5 mV amplitude in the frequency range of 0.01–100 kHz. Fitting of the impedance spectra by the proposed equivalent circuit was performed with Zview2. All the tests were performed at room temperature.

3. Results and discussion

3.1. Characterizations of morphology

The morphologies of the samples were characterized by SEM. Note that after mild oxidation, MCMBO still keeps spherical shape with wrinkles on the surface because of large amount of oxygen-containing groups attached onto the basal or edge plane (Fig. 2a and its inset). Interestingly, a large number of open pores constituted by graphene-like nanoplatelets are observed on the surface of NR-MCMBO (Fig. 2b and its inset). Such porous texture would offer the chemistry and structure to store the lithium ions, and the pore-transport system would ensure the accessibility of those sites by lithium ions [22]. SEM image of the MCMBs obviously shows that it has a spherical shape and its surface is smooth (Supporting Information, Fig. S3a), meanwhile CR-MCMBO shows the similar structure with NR-MCMBO (Fig. S3b and its inset).

3.2. Porous structure

The Brunauer–Emmett–Teller (BET) specific surface area and porous characteristics of CR-MCMBO and NR-MCMBO were investigated by nitrogen adsorption–desorption isotherms (Fig. 3a). The BET specific surface areas of CR-MCMBO and NR-MCMBO are 181.5 and 196.4 $m^2 g^{-1}$, respectively, much higher than that of the pristine MCMBs (0.6 $m^2 g^{-1}$). The large specific surface area is beneficial for electrolyte access. The spherical NR-MCMBO possesses a certain amount of open pores, and possesses a pore volume of 0.36 $cm^3 g^{-1}$ which is nearly three times than that of CR-MCMBO (0.13 $cm^3 g^{-1}$). The pore-size distribution derived from the adsorption branches of isotherms by using the Barrett–Joyner–Halenda model is given in Fig. 3b, showing that both the pore sizes of CR-MCMBO and NR-MCMBO are ranged from 3.5 nm to 4.5 nm (Fig. 3b, inset). It was reported that ion-buffering reservoirs can be formed in the macropores to minimize the diffusion distances to the interior surfaces [23]. The electrolyte in the macropores is similar to those of the bulk electrolyte with the lowest resistance. The unique porous structure may facilitate the diffusion of Li ions to the active sites. As can be seen from Fig. S4, the pore-size of HR-MCMBO is mainly smaller than 2.5 nm and the BET specific surface area is 128 $m^2 g^{-1}$. These values are smaller than that of CR-MCMBO and NR-MCMBO, which may be caused by the formation of internal closed pore during the heat treatment at 800 °C in nonreactive atmosphere of N_2 [24].

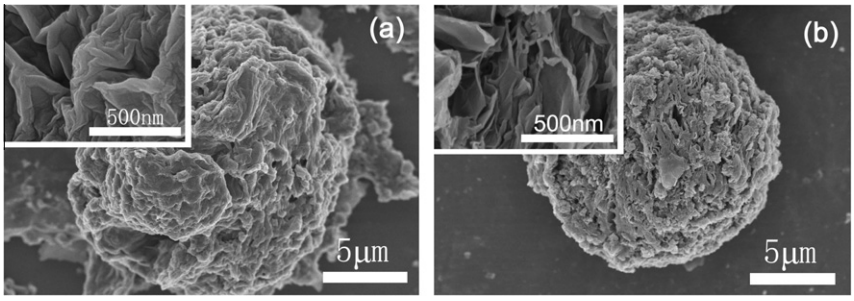

Fig. 2 – SEM images of (a) MCMBO, and (b) NR-MCMBO. The insets in (a) and (b) are its detail view, respectively.

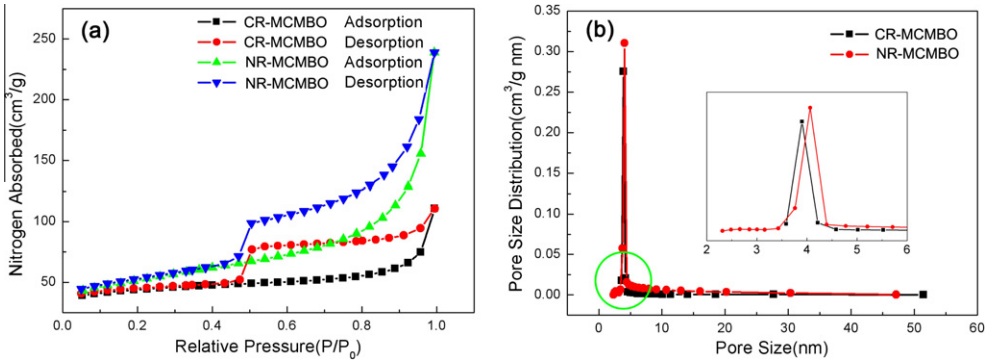

Fig. 3 – (a) Nitrogen sorption isotherms, and (b) BJH pore-size distributions of CR-MCMBO and NR-MCMBO. The inset in (b) is the detailed view of the green circle. (For interpretation of the references to color in this figure legend, the reader is referred to the web version of this article.)

3.3. *Raman spectra, XPS and XRD analyses*

Raman spectra with characteristic G and D bands sensitive to defects and disorder have extensively been used to characterize carbon materials [25,26]. The G band arises from the zone center E_{2g} mode, corresponding to ordered sp^2 bonded carbon, whereas the D band is ascribed to edges, other defects, and disordered carbon. Fig. 4a displays the Raman spectrum of NR-MCMBO. A prominent G band at 1602 cm^{-1} and a typical D band at 1353 cm^{-1} are observed. Nevertheless, the D band is stronger than the G band with an I_D/I_G ratio of 1.12, indicating the presence of a large amount of defects in the graphene layers. The I_D/I_G ratios of CR-MCMBO and HR-MCMBO are 1.06 and 1.02 (Fig. S5), respectively, which indicate the existence of smaller amount of defects. The Raman spectrum of the pristine MCMBs clearly shows that the intensity of D band is much smaller compared to the other samples.

To confirm the successful doping of nitrogen in NR-MCMBO, XPS studies were carried out. The XPS spectrum of NR-MCMBO shows the presence of the principal C1s, O1s and N1s core levels (Fig. 4b), and the atomic percentage of doped nitrogen is calculated to be about 3.8%. As shown in Fig. 4c, the C1s core level peak can be resolved into three components centered at 284.9, 285.8, and 286.9 eV, representing sp^2C-sp^2C, N-sp^2C, and N-sp^3C bonds, respectively. Similarly, the N1s peak can also be resolved into three components centered at 399.3, 400.7, and 402.7 eV, representing pyridinic, pyrrolic, and graphitic type of N atoms doped in the graphene structure (Fig. 4d) [13]. The amount of pyridinic N atoms is estimated to be as high as 51.6% of the total N atoms. As presented in Fig. S6, no N element existed in HR-MCMBO.

The structural changes of MCMBs were investigated by XRD, as shown in Fig. S7. For pristine MCMB, the (002) diffraction peak appeared at 26.61 is strong in intensity and sharp in width. After oxidation and nitrogen doping, the (002) peak is shifted back to 26.50, but its intensity is far smaller than that of the pristine MCMBs, implying that the ordered degree of NR-MCMBO decreased. Crystallite parameters *La* and *Lc* were calculated using the Scherrer equation [27], respectively, as listed in Table S1. It is observed that, *La* and *Lc* of NR-MCMBO decrease rapidly to the values of 21 nm and 9.8 nm, much smaller than that of MCMBs. The result suggests that the stacking height and width of graphite crystallite decreased through oxidation and nitrogen doping. The reduced dimensions can significantly improve the rate capability of lithium insertion/removal, because of the shorten distances for lithium-ion transport within the particles. The characteristic time constant for diffusion is given by $t = L^2/D$, where L is the diffusion length and D the diffusion constant. The time t for diffusion decreases with the reduced diffusion length [28,29].

3.4. *Electrochemical properties*

To investigate the property of the unique NR-MCMBO as anode material of LIBs, electrochemical measurements were carried out. Fig. 5a shows the first CV of the samples conducted at a scan rate of 0.1 mV s^{-1} in 1 mol L^{-1} solution of $LiPF_6$ containing 1:1 (v/v) mixture of EC and DMC as an electrolyte against Li as counter and reference electrode. It can be obviously seen that NR-MCMBO exhibits the largest cathodic/anodic peak area under the same quantity of the active

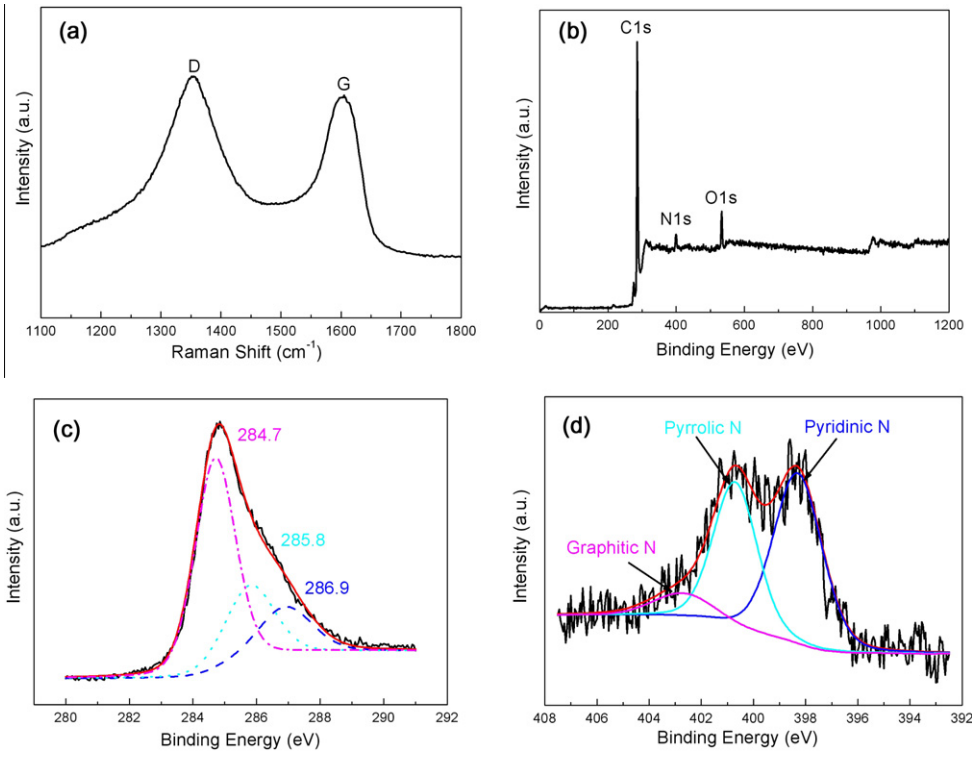

Fig. 4 – (a) Raman spectrum, (b) XPS general spectrum, (c) curve fitting of C1s spectrum, and (d) curve fitting of N1s spectrum of NR-MCMBO.

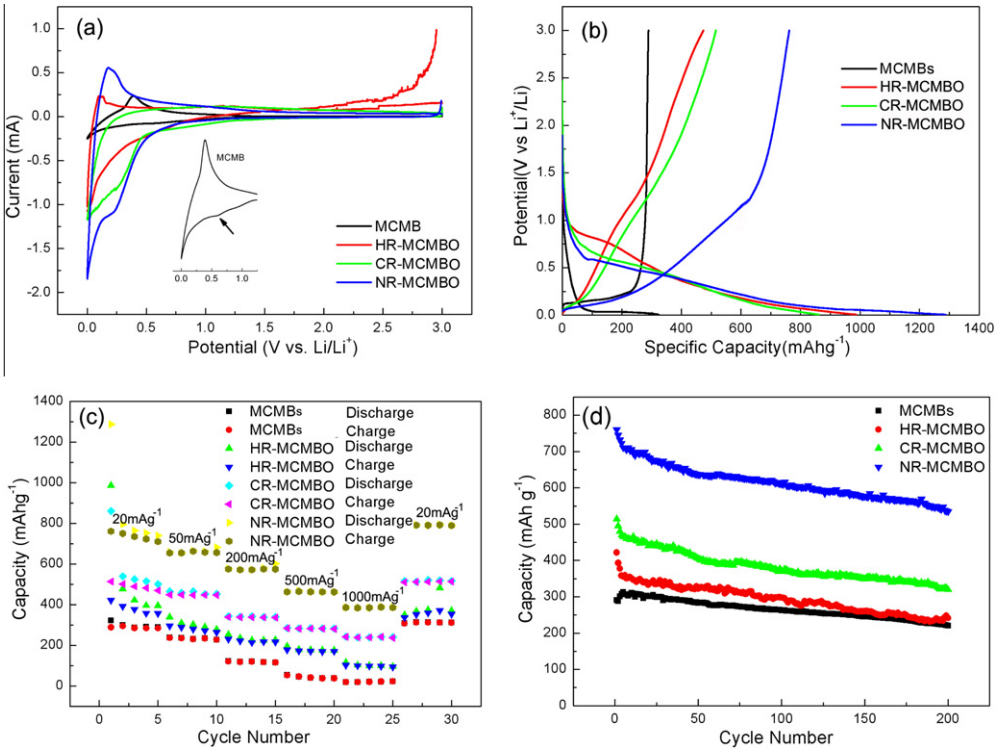

Fig. 5 – Electrochemical performance of NR-MCMBO, CR-MCMBO, HR-MCMBO and MCMBs. (a) CV curves of the samples in 1 mol L^{-1} solution of $LiPF_6$ containing 1:1 (v/v) mixture of EC and DMC as the electrolyte with Li as counter and reference electrode (scan rate: 0.1 mV s^{-1}), inset is the detailed CV view of MCMBs, (b) first charge/discharge profile cycled at a current density of 20 mA g^{-1} between 3 and 0.005 V vs. Li^+/Li, (c) rate capability, and (d) charge capacity verse cycle number at a current density of 20 mA g^{-1} between 3 and 0.005 V vs. Li^+/Li.

material, indicative of the highest Li storage capability. The cathodic peak at 0.3–0.5 V can be attributed to the reaction of lithium ions with the residual oxygen-containing functional groups and the formation of a solid electrolyte interface (SEI) film on the surface of the samples. The SEI film is associated with electrolyte decomposition and the formation of lithium organic compounds. The peak disappears from the second cycle in the all samples (Fig. S8). Fig. 5b shows the first discharge and charge curves of the samples cycled at a rate of 20 mA g^{-1} between 3 and 0.005 V vs. Li^+/Li. For MCMBs, there is a typical Li insertion/extraction profile with a reversible capacity of 289 mAh g^{-1}. HR-MCMBO, CR-MCMBO and NR-MCMBO show similar discharge/charge profiles without distinct potential plateaus [30]. For HR-MCMBO, the first discharge and charge capacities are 998 and 422 mAh g^{-1}, whereas the corresponding capacities for CR-MCMBO are 861 and 514 mAh g^{-1}, respectively. As for NR-MCMBO, the corresponding capacities dramatically increase to 1287 and 762 mAh g^{-1}, respectively, which are much higher than those of the previously reported expanded MCMBs (310 mAh g^{-1}) [31], and metal doped MCMBs (420–462 mAh g^{-1}) [32,33]. The increase of the reversible capacity of NR-MCMBO over MCMBs, HR-MCMBO and CR-MCMBO should be mainly attributed to its high percentage of pyridinic N atoms, as observed in the XPS data. Moreover, the large surface area and abundant internal defects of NR-MCMBO generated by nitrogen-doping further enhance the Li storage properties. The defects at edge sites and internal (basal-plane) defects (vacancies, etc.) of the nanodomains embedded in NR-MCMBO may involve the reversible Li storage because these defects do not come into contact with the electrolyte [34]. As shown in Fig. S9, carbon coated NR-MCMBO delivers the first discharge/charge capacities of 1175 and 825 mAh g^{-1} at the current density of 20 mA g^{-1}, and well maintains the charge capacity at 780 mAh g^{-1} during the following two cycles. The enhanced reversible capacity may be ascribed to the low specific surface area and amorphous carbon structure on the surface [35,36].

The porous structure and N-doping in spherical NR-MCMBO would offer the chemistry and structure to insert and store the lithium ions from different direction, and the pore-transport system would ensure the accessibility of those sites by lithium ions. In addition, the electrical conductivity may be improved when nitrogen is introduced into bulk carbon. The detailed rate capability of the samples is shown in Fig. 5c. Correspondingly, the charge/discharge profiles cycled with different current densities are given in Fig. S10. Compared with other samples, NR-MCMBO illustrates a much better rate performance. In particular, when the current density reaches to 1000 mA g^{-1}, the specific capacity of the NR-MCMBO still retains 388 mAh g^{-1}. However, the capacity of CR-MCMBO decreases to 240 mAh g^{-1} at 1000 mA g^{-1}. As far as MCMBs are concerned, only 20 mAh g^{-1} is retained at 1000 mA g^{-1}. These results clearly show that the porous structure confirmed by nitrogen adsorption–desorption isotherms is favorable for the transport of Li ions and plays an important

role in improving the rate capability. Fig. 5d depicts the charge capacity verse cycle numbers of all samples for 200 cycles. For pristine MCMBs, stable cycling capacity is presented. As for NR-MCMBO, capacity fading takes place for the first few cycles. However, in the subsequent cycles, NR-MCMBO displays good cycle performance, and the specific capacity still maintains 535 mAh g^{-1} after 200 cycles. The unique porous structure and the large amount of defects with nitrogen-doping jointly contribute to the favorable electrochemical performance of NR-MCMBO. Similar result is found in CR-MCMBO with relatively lower capacity compared with NR-MCMBO.

In order to investigate the variation of the volumetric capacity of the electrode, the volumetric capacity was calculated according to Formula (1). As shown in Table 1, the volume of MCMBs loaded on the current collector is the lowest among all of the materials under the same mass. That is to say that the volume becomes higher after Hummers oxidation of MCMBs. Although MCMBs show the smallest gravimetric capacity, its volumetric capacity is higher than of HR-MCMB under the current density of 50 mA g^{-1}. When the current density reaches to 1000 mA g^{-1}, the volumetric capacity of MCMBs decreases to the lowest one. As for NR-MCMBO, its volumetric capacity at 1000 mA g^{-1} still retains 129 mA cm^{-3}, which is half of the value at 50 mA g^{-1}.

3.5. *EIS analysis*

Nyquist plots of the electrodes before cycling and after 5 cycles at charge state (3.0 V vs. Li^+/Li) are shown in Fig. 6. A semicircle at the high-to-medium frequencies and a straight slopping line at low frequencies can be observed before cycling in common. The semicircle represents the charge-transfer resistance, whereas the straight slopping line is associated with the diffusion resistance in the bulk of the active material. Obviously, the charge-transfer resistance of NR-MCMBO electrode is the smallest among all the electrodes before cycling. Simultaneously, it also can be deduced that nitrogen-doping is favorable for electrolyte accessibility. To investigate the influence of nitrogen-doping on electrochemical properties of charge/discharge process, additional Nyquist characterization was carried out after 5 cycles. An equivalent circuit (inset of Fig. 6b) was used to analyze the measured impedance data [37,38], where Rs represents the total resistance of electrolyte, electrode, and separator. R_{SEI} and CPE_1 are the resistance and capacitance of the SEI formed on the electrode, respectively. R_{ct} and CPE_2 represent the charge-transfer resistance and the double layer capacitance, respectively, and Z_w is the Warburg impedance related to the diffusion of lithium ions into the bulk electrode. The fitting values along with this equivalent circuit are presented in Table 2. As can be seen, the R_{SEI} and R_{ct} of NR-MCMBO electrode are 1.72 and 0.78 Ω, respectively, which are much smaller than that of the other three electrodes, indicating that both SEI resistance and charge transfer resistance are significantly reduced through N-doping. That is to say, N-doping is helpful in the formation of the favorable SEI. The well formed porous system of NR-MCMBO facilitates the diffusion of lithium ions into the bulk electrode.

Table 1 – Volumetric capacity of the electrode calculated according to Formula (1) under the current density of 50 and 1000 mA g^{-1}.

Samples	Gravimetric capacity (mAh g^{-1})		M (g)[a]	V (cm^3)[b]	Volumetric capacity (mAh cm^{-3})	
	50 mA g^{-1}	1000 mA g^{-1}			50 mA g^{-1}	1000 mA g^{-1}
MCMBs	289	20	3.2×10^{-3}	6.3×10^{-3}	146	10
HR-MCMBO	422	94	3.2×10^{-3}	9.4×10^{-3}	143	32
CR-MCMBO	514	240	3.2×10^{-3}	1.0×10^{-2}	164	76
NR-MCMBO	762	388	3.2×10^{-3}	9.6×10^{-3}	254	129

a Mass of active materials.
b Volume of active materials.

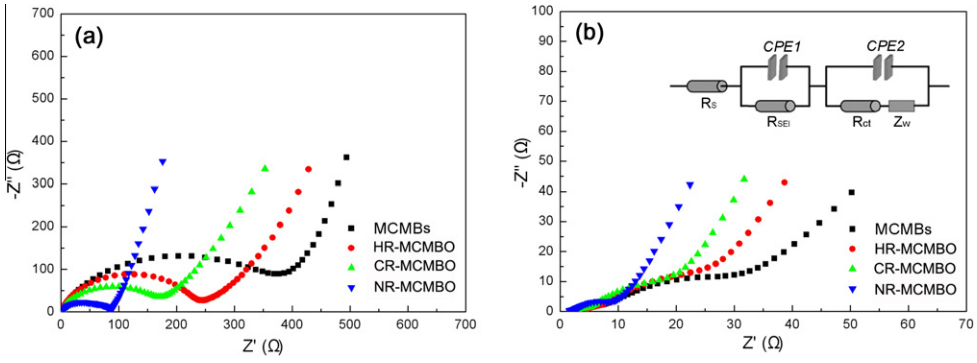

Fig. 6 – Nyquist plots for the electrodes at 3.0 V (vs. Li^+/Li): (a) before cycling, and (b) Nyquist plots for the electrodes after 5 cycles (inset is the equivalent circuit used to fit experimental curves).

Table 2 – Values of the equivalent circuit components obtained by fitting the experimental curves.

Components	Fitted values			
	MCMBs	HR-MCMBO	CR-MCMBO	NR-MCMBO
R_s (Ω)	2.94	2.40	2.90	2.55
R_{SEI} (Ω)	2.15	2.93	2.86	1.72
CPE_1 (F)	3.08E−5	7.04E−5	1.49E−4	1.14E−4
R_{ct} (Ω)	4.51	2.18	1.51	0.78
CPE_2 (F)	1.56E−6	1.39E−6	1.49E−6	5.86E−6

4. Conclusions

In this work, NR-MCMBO was fabricated through nitrogen-doping in CR-MCMBO by simple annealing in ammonia, and was also studied as an anode material of LIBs. NR-MCMBO exhibits significantly enhanced the reversible capacity in comparison with the pristine MCMBs, which should be attributed to the high amount of pyridinic nitrogen, defects at edge sites and internal defects presented in NR-MCMBO. Additionally, the pore-transport system constituted by graphene-like nanoplatelets in spherical NR-MCMBO ensures the accessibility for lithium ions, which greatly improve the rate capability, volumetric capacity and cycle performance. Nitrogen-doping into CR-MCMBO makes it a feasible process to improve the lithium ion storage capability of MCMBs, and is beneficial to the application as anode material of LIBs.

Acknowledgements

We appreciate the support of “100 Talents” program of the Chinese Academy of Sciences, National Key Basic Research Program of China (Grant No. 2011CB935700), Shandong Province Funds for Distinguished Young Scientist (Grant No. JQ200906) and National Natural Science Foundation of China (Grant No. 20971077).

Appendix A. Supplementary data

Supplementary data associated with this article can be found, in the online version, at doi:10.1016/j.carbon.2011.11.007.

REFERENCES

[1] Tarascon JM, Armand M. Issues and challenges facing rechargeable lithium batteries. Nature 2001;414(6861):359–67.
[2] Armand M, Tarascon JM. Building better batteries. Nature 2008;451(7179):652–7.
[3] Goodenough JB, Kim Y. Challenges for rechargeable Li batteries. Chem Mater 2010;22(3):587–603.
[4] Dahn JR, Zheng T, Liu YH, Xue JS. Mechanisms for lithium insertion in carbonaceous materials. Science 1995;270(5236):590–3.
[5] Cui GL, Zhi LJ, Thomas A, Kolb U, Lieberwirth I, Müllen K. One-dimensional porous carbon/platinum composites for nanoscale electrodes. Angew Chem Int Ed 2007;46(19):3464–7.
[6] Winter M, Besenhard JO, Spahr ME, Novák P. Insertion electrode materials for rechargeable lithium batteries. Adv Mater 1998;10(10):725–63.
[7] Li JX, Wu CX, Guan LH. Lithium insertion/extraction properties of nanocarbon materials. J Phys Chem C 2009;113(42):18431–5.
[8] Wu XL, Chen LL, Xin S, Yin YX, Guo YG, Kong QS, et al. Preparation and Li storage properties of hierarchical porous carbon fibers derived from alginic acid. ChemSusChem 2010;3(6):703–7.
[9] Yang SB, Feng XL, Zhi LJ, Cao Q, Maier J, Müllen K. Nanographene-constructed hollow carbon spheres and their favorable electroactivity with respect to lithium storage. Adv Mater 2010;22(7):838–42.
[10] Cui GL, Gu L, Thomas A, Fu LJ, Aken PA, Antonietti M, et al. A carbon/titanium vanadium nitride composite for excellent lithium storage properties. ChemPhysChem 2010;11(15):3219–23.
[11] Wu YP, Jiang CY, Wan CR, Fang SB, Jiang YY. Nitrogen-containing polymeric carbon as anode material for lithium ion secondary battery. J Appl Polym Sci 2000;77(8):1735–41.
[12] Ayala P, Arenal R, Rümmeli M, Rubio A, Pichler T. The doping of carbon nanotubes with nitrogen and their potential applications. Carbon 2010;48(3):575–86.
[13] Reddy AL, Srivastava A, Gowda SR, Gullapalli H, Dubey M, et al. Synthesis of nitrogen-doped graphene films for lithium battery application. ACS Nano 2010;4(11):6337–42.
[14] Wang HB, Zhang CJ, Liu ZH, Wang L, Han PX, Xu HX, et al. Nitrogen-doped graphene nanosheets with excellent lithium storage properties. J Mater Chem 2011;21(14):5430–4.
[15] Dokko K, Nakata N, Suzuki Y, Kanamura K. High-rate lithium deintercalation from lithiated graphite single-particle electrode. J Phys Chem C 2010;114(18):8646–50.
[16] Wang GX, Yao J, Liu HK. Characterization of nanocrystalline Si-MCMB composite anode materials. Electrochem Solid-State Lett 2004;7(8):A250–3.
[17] Courtel FM, Niketic S, Duguay D, Abu-Lebdeh Y, Davidson IJ IJ. Water-soluble binders for MCMB carbon anodes for lithium-ion batteries. J Power Sources 2011;196(4):2128–34.
[18] Norfolk C, Mukasyan A, Hayes D, McGinn P, Varma A. Processing of mesocarbon microbeads to high-performance materials: Part I. Studies towards the sintering mechanism. Carbon 2004;42(1):11–9.
[19] Norfolk C, Mukasyan A, Hayes D, McGinn P, Varma A. Processing of mesocarbon microbeads to high-performance materials: Part III. High-temperature sintering and graphitization. Carbon 2006;44(2):301–6.
[20] William S, Hummers W, Offman R. Preparation of graphitic oxide. J Am Chem Soc 1958;80(6):1339.
[21] Nethravathi C, Rajamathi M. Chemically modified graphene sheets produced by the solvothermal reduction of colloidal dispersions of graphite oxide. Carbon 2008;46(14):1994–8.
[22] Hu YS, Adelhelm P, Smarsly BM, Hore S, Antonietti M, Maier J. Synthesis of hierarchically porous carbon monoliths with highly ordered microstructure and their application in rechargeable lithium batteries with high-rate capability. Adv Funct Mater 2007;17(12):1873–8.
[23] Wang DW, Li F, Liu M, Lu GQ, Cheng HM. 3D aperiodic hierarchical porous graphitic carbon material for high-rate

electrochemical capacitive energy storage. Angew Chem Int Ed 2008;47(2):73–6.
[24] Hanzawa Y, Hatori H, Yoshizawa N, Yamada Y. Structural changes in carbon aerogels with high temperature treatment. Carbon 2002;40(4):575–81.
[25] Chen WF, Yan LF, Bangal PR. Preparation of graphene by the rapid and mild thermal reduction of graphene oxide induced by microwaves. Carbon 2010;48(4):1146–52.
[26] Shen JF, Hu YZ, Shi M, Lu X, Qin C, Li C, et al. Fast and facile preparation of graphene oxide and reduced graphene oxide nanoplatelets. Chem Mater 2009;21(15):3514–20.
[27] Fukuda K, Kikuya K, Isono K, Yoshio M. Foliated natural graphite as the anode material for rechargeable lithium-ion cells. J Power Source 1997;69(1–2):165–8.
[28] Bruce PG, Scrosati B, Tarascon JM. Nanomaterials for rechargeable lithium batteries. Angew Chem Int Ed 2008;47(16):2930–46.
[29] Maier J. Size effects on mass transport and storage in lithium batteries. J Power Sources 2007;174(2):569–74.
[30] Guo P, Song HH, Chen XH. Electrochemical performance of graphene nanosheets as anode material for lithium-ion batteries. Electrochem Commun 2009;11(6):1320–4.
[31] Yang SB, Song HH, Chen XH. Electrochemical performance of expanded mesocarbon microbeads as anode material for lithium-ion batteries. Electrochem Commun 2006;8(1):137–42.
[32] Wang GX, Yao J, Liu HK, Dou SX, Ahn JH. Electrochemical characteristics of tin-coated MCMB graphite as anode in lithium-ion cells. Electrochim Acta 2004;50(2-3):517–22.
[33] Shi LH, Li H, Wang ZX, Huang XJ, Chen LQ. Nano-SnSb alloy deposited on MCMB as an anode material for lithium ion batteries. J Mater Chem 2001;11(5):502–5.
[34] Pan DY, Wang S, Zhao B, Wu MH, Zhang HJ, Wang Y, et al. Li storage properties of disordered graphene nanosheets. Chem Mater 2009;21(14):3136–42.
[35] Zhang HL, Liu SH, Li F, Bai S, Liu C, Tan J, et al. Electrochemical performance of pyrolytic carbon-coated natural graphite spheres. Carbon 2006;44(11):2212–8.
[36] Nozaki H, Nagaoka K, Hoshi K, Ohta N, Inagaki M. Carbon-coated graphite for anode of lithium ion rechargeable batteries: carbon coating conditions and precursors. J Power Sources 2009;194(1):486–93.
[37] Kamisah MM, Munirah HS, Mansor MS. Electrochemical impedance study of lithium-ion insertion into rice husk carbon. Ionics 2007;13(4):223–5.
[38] Zhang S, Shi PF. Electrochemical impedance study of lithium intercalation into MCMB electrode in a gel electrolyte. Eletrochim Acta 2004;49(9-10):1475–82.